Electronic Properties of Mixed-Valence Manganates: The Role of Mn Substitutional Defects

Zoubaïda El-Fadli,† M. Redouane Metni,† Fernando Sapiña,* Eduardo Martinez, José-Vicente Folgado, and Aurelio Beltrán

Institut de Ciència dels Materials de la Universitat de València, Apartado de Correos 2085, E-46071 València, Spain

Received July 9, 2001. Revised Manuscript Received November 12, 2001

Single-phase perovskites in the solid solution series $La_{0.7+y}A_{0.3-y}Mn_{1-x}M_xO_3$ (with $0.00 \leq x \leq 0.10$; A = Sr^{2+}, M = Cu^{2+}, Zn^{2+}, Sc^{3+}, Cr^{3+}, Co^{3+}, and Ga^{3+}; A = Ba^{2+}, M = Cu^{2+}, Zn^{2+}, and Sc^{3+}) have been prepared via the acetic acid solutions freeze-drying method. This soft procedure makes possible strict stoichiometric control, and the synthetic variables allow one to maintain a constant proportion of Mn^{4+} (ca. 32%) in the 47 compounds prepared. In this way, the concentration of cationic vacancies at A and B sites is practically negligible in all cases. X-ray powder diffraction patterns corresponding to the 47 compounds have been completely indexed with rhombohedral perovskite cells. The crystal structures have been refined in space group $\bar{R}3c$, in the hexagonal setting, from room-temperature data. The variation with x of a set of structural parameters (rhombohedral cell volume, rhombohedral cell angle, and B−O and A−O bond lengths) has been considered as a function of the mean sizes of cations at A and B sites. Manganates in these series present colossal magnetoresistance. The values of the critical temperature, T_c, for the paramagnetic−ferromagnetic transition in $La_{0.7+y}A_{0.3-y}Mn_{1-x}M_xO_3$ exhibit three different patterns, which clearly appear related to the mean size of cations at B sites. This fact has been interpreted by considering the variation of the electronic contribution to T_c with the structural disorder introduced by the presence of cations with different sizes at B sites.

Introduction

Interest in doped rare-earth manganates has been on the rise in recent years because of the discovery of colossal magnetoresistance (CMR) in $Ln_{1-x}A_xMnO_{3\pm\delta}$ (Ln = La, Pr, Nd, and Sm; A = Ca, Sr, and Ba) perovskites.[1] In fact, the electronic properties of these types of oxides attracted attention long before the observation of the associated CMR effects,[2] and they have been widely investigated for technological applications.[3] After CMR discovery, the possibility of tailoring the physical properties of these mixed-valence manganates became a challenge. This has resulted in a great deal of work intended to understand the basic aspects of the mechanisms of interaction between manganese ions that give rise to the observed large magnetoresistance.

In light of the currently available results, CMR appears as a multivariable intricate phenomenon whose understanding in terms of a satisfactory model requires further systematic investigations. A first remarkable result was the observation of the relevance for CMR of the mean oxidation state of the manganese ions, with an optimum value (i.e., that leading to a maximum value of the critical temperature for the paramagnetic−ferromagnetic transition, T_c) close to 3.3.[4] Studies on $Ln_{0.7}A_{0.3}MnO_3$ samples with such a concentration (ca. 30%) of Mn^{4+} also showed the existence of a certain relationship between T_c and the structural distortion of the perovskite structure as measured by the tolerance factor, t, or the mean size of cations at the A sites, $\langle r_A \rangle$.[5] More recent studies on related $Ln_{0.7}A_{0.3}MnO_3$ samples have shown that, in perovskite series with a fixed $\langle r_A \rangle$ value, T_c depends on the disorder at the A sites [as represented by the variance of the A cationic radii distribution, $\sigma^2(\langle r_A \rangle)$].[6]At this point, it should be noted that there is evidence about the dependence of the critical temperature and phase diagram of $Ln_{0.5}A_{0.5}MnO_3$ and the critical temperature of $(Ln_{1-x}A_x)_2CuO_4$

* To whom correspondence should be addressed. E-mail: fernando.sapina@uv.es. Phone: 34-96-3983626. Fax: 34-96-3983633.
† Permanent address: Département de Chimie, Faculté des Sciences, Université Abdelmalek Essaadi, Tétouan, Morocco.

(1) (a) Kusters, R. M.; Singleton, J.; Keen, D. A.; McGreevy, R.; Hayes, W. *Phys. B* **1989**, *155*, 362. (b) von Helmot, R.; Wecker, J.; Holzapfel, B.; Schultz, L.; Samwer, K. *Phys. Rev. Lett.* **1993**, *71*, 2331. (c) Jin, S.; Tiefel, T. H.; McCormack, M.; Fastnacht, R. A.; Ramesh, R. L.; Chen, H. *Science* **1994**, *64*, 413.

(2) (a) Zener, Z. *Phys. Rev.* **1951**, *82*, 403. (b) Anderson, P. W. *Phys. Rev.* **1955**, *100*, 675. (c) De Gennes, P. G. *Phys. Rev.* **1960**, *116*, 141.

(3) (a) Tejuca, L. G.; Fierro, J. L.; Tascón, J. M. D. *Adv. Catal.* **1989**, *36*, 237 and references therein. (b) Minh, N. Q. *J. Am. Ceram. Soc.* **1993**, *76*, 563 and references therein. (c) Hellemans, A. *Science* **1996**, *273*, 880.

(4) (a) Schiffer, P.; Ramirez, A. P.; Bao, W.; Cheong, S. W. *Phys. Rev. Lett.* **1995**, *75*, 3336. (b) Urushibara, A.; Moritomo, Y.; Arima, T.; Asamitsu, A.; Kido, G.; Tokura, Y. *Phys. Rev. B* **1995**, *51*, 14103.

(5) (a) Maignan, A.; Caignert, V.; Simon, Ch.; Hervieu, M.; Raveau, B. *J. Mater. Chem.* **1995**, *5*, 1091. (b) Hwang, H. Y.; Cheong, S. W.; Radaelli, P. G.; Marezio, M.; Batlogg, B. *Phys. Rev. Lett.* **1995**, *75*, 914. (c) Mahesh, R.; Mahendiran, R.; Raychaudhuri, A. K.; Rao, C. N. R. *J. Solid State Chem.* **1995**, *120*, 204. (d) Fontcuberta, J.; Martinez, B.; Piñol, S.; García-Muñoz, J. L.; Obradors, X. *Phys. Rev. Lett.* **1996**, *76*, 1122.

(6) (a) Rodriguez-Martinez, L. M.; Attfield, J. P. *Phys. Rev. B* **1996**, *54*, R15622. (b) Rodriguez-Martinez, L. M.; Attfield, J. P. *Phys. Rev. B* **1998**, *58*, 2426. (c) Attfield, J. P. *Chem. Mater.* **1998**, *10*, 3239.

10.1021/cm010655e CCC: $22.00
Published on Web 02/01/2002

superconductors with $\langle r_A \rangle$ and $\sigma^2(\langle r_A \rangle)$.[6c,7,8] Other factors, such as the electronegativity[9] and the magnetic moments of ions at the A sites,[10] have also been described as influencing the electronic properties of these types of materials. However, we have recently shown that it is the disorder at A sites (and not the electronegativity of cations at A sites) that determines the electronic properties of samples in the $La_{0.85}(Na_{1-x}K_x)_{0.15}MnO_3$ series.[11]

There is comparatively less information concerning effects associated with the presence of different defects in the B cationic sublattice. In some cases, mixed-valence manganese perovskites present oxygen nonstoichiometry, which is accommodated in the lattice as cation vacancies.[12] The study of the solid solution series $La_{1-x}A_xMnO_{3+\delta}$ (A = Na, K; $0 \le x \le 0.15$) allowed us to show how the electronic properties of mixed-valence manganates with a similar concentration of holes (close to the optimum value) are controlled by the concentration of vacancies at B sites.[13] The B cationic perovskite sublattice also can be altered through Mn-site doping by other cations, i.e., by preparing $Ln_{1-y}A_yMn_{1-x}M_xO_{3+\delta}$ manganates. Special attention has been payed in this case to the influence of the substitutions on the charge-ordered ground state (i.e., to perovskites having 50% Mn^{4+}).[14] However, there are fewer results concerning Mn-substituted perovskites having the optimum content of Mn^{4+} (ca. 30%). Although T_c decreases after Mn substitution depending on the nature and concentration of the dopant element, there is not yet enough data to correlate the dependence of T_c with any fundamental variable.[15]

We report here new results from a systematic study on $La_{0.7+y}A_{0.3-y}Mn_{1-x}M_xO_3$ (with $0.00 \le x \le 0.10$; A = Sr^{2+}, M = Cu^{2+}, Zn^{2+}, Sc^{3+}, Cr^{3+}, Co^{3+}, and Ga^{3+}; A = Ba^{2+}, M = Cu^{2+}, Zn^{2+}, and Sc^{3+}) manganates having a constant proportion of Mn^{4+} (ca. 32%). As shown below, the size of the substitutional M defects is a key factor regarding T_c values in this family of mixed-valence manganates. We subsequently propose a model that allows us not only to rationalize this fact but also to explain how the presence of vacancies at B sites of the perovskite structure modifies T_c.

Table 1. Chemical Analysis for Samples of Nominal Composition $La_{1-y}A_yMn_{1-x}M_xO_3$[a,b]

	$x = 0.00$	$x = 0.02$	$x = 0.04$	$x = 0.06$	$x = 0.08$	$x = 0.10$
			A = Sr; M = Cr			
y	0.30	0.294	0.288	0.282	0.276	0.270
% Mn^{4+}	31	32	31	31	31	31
δ	0.005	0.010	0.005	0.005	0.005	0.005
			A = Sr; M = Co			
y		0.294	0.288	0.282	0.276	0.270
% Mn^{4+}		30	30	31	31	31
δ		0	0	0.005	0.005	0.005
			A = Sr; M = Ga			
y		0.294	0.288	0.282	0.276	0.270
% Mn^{4+}		31	31	33	32	34
δ		0.005	0.005	0.014	0.010	0.018
			A = Sr; M = Cu			
y		0.274	0.248	0.222	0.196	0.170
% Mn^{4+}		32	32	32	35	32
δ		0.010	0.010	0.010	0.023	0.010
			A = Sr; M = Zn			
y		0.274	0.248	0.222	0.196	0.170
% Mn^{4+}		30	31	33	32	33
δ		0	0.005	0.014	0.010	0.014
			A = Sr; M = Sc			
y		0.294	0.288	0.282	0.276	0.270
% Mn^{4+}		31	31	31	32	33
δ		0.005	0.005	0.005	0.010	0.014
			A = Ba; M = Cu			
y	0.30	0.274	0.248	0.222	0.196	0.170
% Mn^{4+}	31	31	31	33	30	32
δ	0.005	0.005	0.005	0.014	0	0.010
			A = Ba; M = Zn			
y		0.274	0.248	0.222	0.196	0.170
% Mn^{4+}		32	31	31	32	32
δ		0.010	0.005	0.005	0.010	0.010
			A = Ba; M = Sc			
y		0.294	0.288	0.282	0.276	0.270
% Mn^{4+}		31	30	31	31	32
δ		0.005	0	0.005	0.005	0.010

[a] Estimated errors in the Mn/La ratios are 0.01. [b] Estimated error in % Mn^{4+}, ±1%.

Experimental Section

Aqueous solutions of metal acetates with molar nominal compositions La:A:Mn:M = $(1 - y):y:(1 - x):x$ (A = Sr, M = Cr, Co, Ga, Sc, Cu, and Zn; A = Ba, M = Sc, Cu, and Zn), where x varies from 0.00 until 0.10 (as indicated in Table 1), were prepared as follows. $SrCO_3$ or $BaCO_3$ was dissolved in a mixture of 100 mL of glacial acetic acid and 20 mL of H_2O. Addition of La_2O_3 led to a suspension, which was gently heated with stirring until a transparent solution was obtained (15 min). After cooling, $Mn(CH_3COO)_2 \cdot 4H_2O$ was added and dissolved upon stirring. Then, the sources of the different metal ions were added (solid sources were $Cr(NO_3)_3 \cdot 9H_2O$ or $M(CH_3COO)_2 \cdot nH_2O$, where M = Co, Cu, and Zn; liquid sources were prepared by dissolving Ga_2O_3 or Sc_2O_3 in the minimum volume of concentrated nitric acid). Values of y were selected for each value of x and dopant metal charge in order to have a constant $[Mn^{4+}]/([Mn^{3+}] + [Mn^{4+}]) = 0.3$ ratio, according to the nominal stoichiometry (see Table 1). The masses of the different reagents were adjusted to give 5 g of perovskite. Droplets of the resulting acetic acid solutions were flash frozen by projection on liquid nitrogen and then freeze-dried at a pressure of 10^{-4} atm. In this way, dried solid precursors were obtained as loose powders. These precursors were heated at 750 °C (12 h,

(7) (a) Damay, F.; Martin, C.; Maignan, A.; Raveau, B. *J. Appl. Phys.* **1997**, *82*, 6181. (b) Raveau, B.; Maignan, A.; Martin, C.; Hervieu, M. *Chem. Mater.* **1998**, *10*, 2641.
(8) Attfield, J. P.; Kharlanov, A. L.; McAllister, J. A. *Nature* **1998**, *394*, 157.
(9) Fontcuberta, J.; Martinez, B.; Piñol, S.; García-Muñoz, J. L.; Obradors, X. *Phys. Rev. B* **1997**, *55*, R668.
(10) Xu, J.; Tang, W. H.; Liang, J. K. *J. Phys.*: *Condes. Matter* **1998**, *10*, 1387.
(11) El-Fadli, Z.; Coret, E.; Sapiña, F.; Martínez, E.; Beltrán, A.; Beltrán, D. *J. Mater. Chem*, **1999**, *8*, 1793.
(12) Töpfer, J.; Goodenough, J. B. *J. Solid State Chem.* **1997**, *130*, 117.
(13) (a) Ng-Lee, Y.; Sapiña, F.; Martínez-Tamayo, E.; Folgado, J. V.; Ibañez, R.; Beltrán, D.; Lloret, F.; Segura, A. *J. Mater. Chem.* **1997**, *7*, 1905. (b) Boix, T.; Sapiña, F.; El-Fadli, Z.; Martínez, E.; Beltrán, A.; Vergara, J.; Ortega, R. J.; Rao, K. V. *Chem. Mater.* **1998**, *19*, 1569. (c) Vergara, J.; Ortega-Hertogs, R. J.; Madurga, V.; Sapiña, F.; El-Fadli, Z.; Martínez, E.; Beltrán, A.; Rao, K. V. *Phys. Rev. B* **1999**, *60*, 1127.
(14) Maignan, A.; Damay, F.; Barnabe, A.; Martin, C.; Hervieu, M.; Raveau, B. *Philos. Trans. R. Soc. A* **1998**, *356*, 1635 and references therein.
(15) (a) Gayathri, N.; Raychaudhuri, A. K.; Tiwary, S. K.; Gundakaram, R.; Arulaj, A.; Rao, C. N. R. *Phys. Rev. B* **1997**, *56*, 1345. (b) Rubinstein, M.; Gillespie, D. J.; Snyder, J. E.; Tritt, T. M. *Phys. Rev. B* **1997**, *56*, 5412. (c) Blasco, J.; García, J.; de Teresa, J. M.; Ibarra, M. R.; Perez, J.; Algarabel, P. A.; Marquina, C. *Phys. Rev. B* **1997**, *55*, 8905. (d) Blanco, J. J.; Lezama, L.; Insausti, M.; Gutiérrez, J.; Barandiarán, J. M.; Rojo, T. *Chem. Mater.* **1999**, *11*, 3463. (e) Gutiérrez, J.; Peña, A.; Barandiarán, J. M.; Pizarro, J. L.; Hernández, T.; Lezama, L.; Insausti, M.; Rojo, T. *Phys. Rev. B* **2000**, *61*, 9028. (f) Gutiérrez, J.; Peña, A.; Barandiarán, J. M.; Pizarro, J. L.; Lezama, L.; Insausti, M.; Rojo, T. *J. Phys.*: *Condens. Matter* **2000**, *12*, 10523.

air flow), and the resulting samples were ground, pelletized, and heated in air at 1150 °C for 48 h.[16]

Lanthanum and manganese contents were determined by atomic absorption using a Perkin-Elmer 300 AA spectrophotometer. Metal ratios in a wide set of selected samples were determined by energy-dispersive analysis of X-rays (EDAX) on a JEOL JSM 6300 scanning electron microscope collected by an Oxford detector, with quantification performed using virtual standards on associated Link-Isis software. The operating voltage was 20 kV, and the energy range for analysis was 0−20 keV. Under these conditions, the lateral resolution of the system was around 1 μm. The results indicate that there is no significant deviation from the nominal cationic stoichiometry. The mean oxidation state of manganese ions, and thus the oxygen content, was determined by redox back-titration of Fe(II) with potassium dichromate in HCl using a Crison CompacT titrator. Summarized in Table 1 are the results of these analyses.

Powder diffraction patterns were obtained with a Seifert C-3000 $\theta-\theta$ automated diffractometer, using graphite-monochromated Cu Kα radiation. The samples were dusted through a sieve on the holder surface. Routine patterns for phase identification were collected with a scanning step of 0.08° 2Θ over the angular range 10−70° 2Θ with a collection time of 3 s/step. For Rietveld analysis, patterns were collected with a scanning step of 0.02° 2Θ, over a wider angular range (20−100° 2Θ), and with a longer acquisition time (greater than 10 s/step) in order to enhance statistics. X-ray data analyses were performed using the FULLPROF program.[17] Graphical representations concerning X-ray powder diffraction patterns were performed using the DRXWin program.[18]

Magnetization measurements were performed in a Quantum Design superconducting quantum interference device magnetometer in the temperature range 5−300 K at 1 T. Isothermal magnetization measurements at 5 K were performed while working with magnetic fields up to 1.0 T. Transition temperatures (T_c) were determined by ac susceptometry measurements performed using a Lake Shore Cryotonics Inc. model 7000 ac susceptometer (temperature range 100−325 K, frequency 333 Hz, exciting field 1 Oe, $T_c \leq 325$ K) or by thermogravimetric experiences, carried out using a Perkin-Elmer 7 system, with the samples under a small magnetic field generated by a magnet ($325 \leq T_c$).[19]

Results

Chemical and Structural Characterization. Freeze-drying of acetic acid solutions has already proven to be a very versatile method for obtaining stoichiometrically controlled manganate perovskites.[11,13,20] Chemical analyses and EDAX results show that there is no significant deviation from the nominal cationic stoichiometry. Then, we have calculated (from the redox back-titration results) the mean oxidation state of manganese ions assuming that the nominal stoichiometry is preserved in all of the products. As pointed out in Table 1, the manganese mean oxidation state is practically constant along the entire series, being 3.32 ± 0.01. As a consequence, δ (oxygen nonstoichiometry) is practically zero ($\delta \leq 0.025$) in all cases, and the concentration of vacancies at the A and B positions is negligible.

X-ray powder diffraction patterns (shown in Figure 1 for the $La_{1-y}Sr_yMn_{1-x}Cu_xO_3$ series) have been completely indexed in the rhombohedral perovskite-type structure. The structures of the perovskite phases have been refined in space group $R\bar{3}c$, in the hexagonal setting, from room-temperature data. The initial structural model used was that of $La_{0.95}Mn_{0.95}O_3$.[21] The fits were performed using a pseudo-Voigt peak-shape function. In the final runs, the usual profile parameters (scale factors, background coefficients, zero points, half-width, pseudo-Voigt, and asymmetry parameters for the peak shape) and atomic positions were refined. Isotropic thermal parameters were set at 0.3 and 0.7 Å^2 for metal and oxygen atoms, respectively, and an overall thermal parameter was also refined. In the structural models, La, Sr, and Ba, and Mn and M are considered to be randomly distributed in the A and B sites, respectively, and their occupancies were fixed to give the metal nominal stoichiometry and the oxygen content obtained from chemical analyses.

Magnetic Properties. We have measured hysteresis loops M(5 K, H) with fields up to 10 kOe, after cooling in a zero magnetic field. The knee of magnetization is reached at 2000 Oe, above that the magnetization changes linearly with the field. Linear extrapolation at $H = 0$ enabled us to derive the spontaneous magnetization, M_S(5 K). In all samples the observed spontaneous magnetization is very close to the theoretical spontaneous magnetization.

The temperature dependence of the magnetization was measured at a field of 10 kOe during warming runs, at temperatures ranging from 5 to 300 K. The curves are presented in Figure 2 for the A = Sr, M = Cu series. The magnetization decreases as the temperature increases. It presents an abrupt drop, which corresponds to the transition from ferromagnetic to paramagnetic states, only in the case of samples for which the transition temperature is lower than 300 K.

The ferromagnetic phase transition temperatures were determined either by means of thermogravimetric experiences performed under a small magnetic field ($T_c \geq 325$ K; the weight variation reflects, then, the variation of the magnetization with the temperature and allows the determination of T_c)[19] or by alternation of susceptometry measurements ($T_c \leq 325$ K). Figure 3 shows the evolution of the normalized force with the temperature for samples in the $La_{1-y}Sr_yMn_{1-x}Cr_xO_3$ series. Such curves are indicative of the accuracy of the thermogravimetric method. These results are summarized in Table 2.

Figure 4 shows the variation of T_c with x for the 47 compounds studied in this work. As can be observed, the results referring to strontium derivatives reveal two different types of behavior. Indeed, when M = Cr^{3+}, Co^{3+}, and Ga^{3+}, the decrease of T_c with x is nearly linear and relatively small (the maximum total T_c decrease,

(16) $La_{0.7}Ba_{0.3}MnO_3$ and samples in the series $La_{0.7}(Ca_{1-x}Sr_x)_{0.3}MnO_3$ (with x = 0.0, 0.2, 0.4, 0.6, 0.8, and 1.0), which are used for comparison, were obtained by using the same preparative procedure.

(17) Rodriguez-Carvajal, J. FULLPROF: A Program for Rietveld Refinement and Pattern Matching Analysis. *Abstracts of the Satellite Meeting on Powder Diffraction of the XV Congress of the IUCr*, Toulouse, France, 1990; p 127.

(18) Primo, V. DRXWin & CreaFit version 2.0: graphical and analytical tools for powder XRD patterns. *Powder Diffr.* **1999**, *14*, 70.

(19) Transition temperatures for $La_{0.7}Ba_{0.3}MnO_3$ and samples in the series $La_{0.7}(Ca_{1-x}Sr_x)_{0.3}MnO_3$ were also obtained by thermogravimetric experiments, except for the x = 0.0 and 0.2 samples (which have transition temperatures lower than 300 K). In these last cases, the transition temperatures were determined by ac susceptibility measurements. All of the experimental results concerning these compounds are in good agreement with those previously reported in the literature for analogous compositions (ref 5).

(20) El-Fadli, Z.; Metni, M. R.; Sapiña, F.; Martínez, E.; Folgado, J. V.; Beltrán, D.; Beltrán, A. *J. Mater. Chem.* **2000**, *10*, 437.

(21) Van Roosmalen, J. A. M.; Cordfunke, E. H. P.; Helmholdt, R. B.; Zandbergen, H. W. *J. Solid State Chem.* **1994**, *110*, 100.

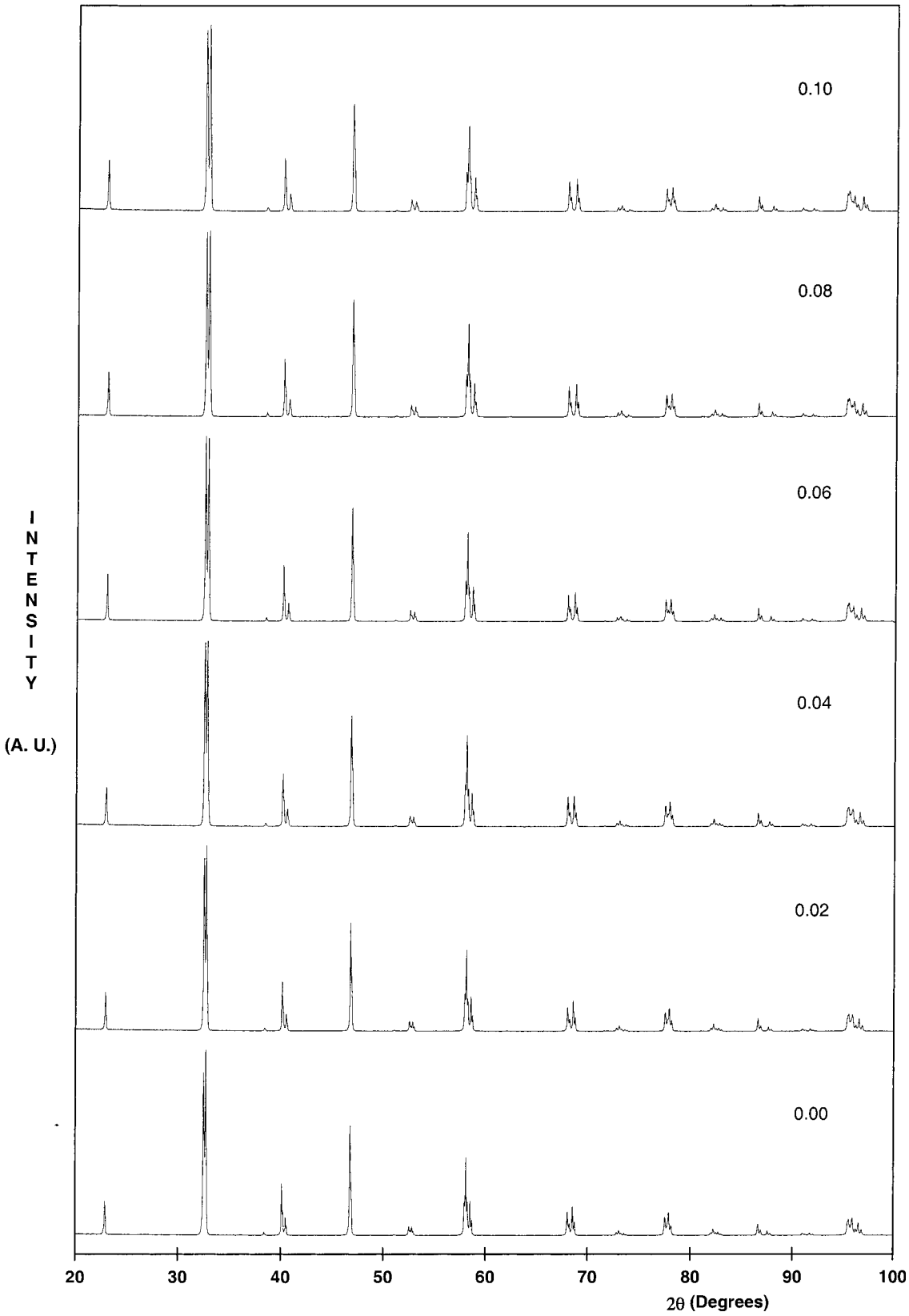

Figure 1. X-ray powder diffraction patterns of $La_{0.7+y}A_{0.3-y}Mn_{1-x}Cu_xO_3$.

19%, is observed for Co^{3+}). In these series, the ionic radii of the dopant cations (Cr^{3+}, 75.5 pm; Co^{3+}, 75 pm; Ga^{3+}, 76 pm) are similar to the mean radius for Mn ions (75.05 pm; calculated as the weighted average value of the ionic radii of Mn^{3+} and Mn^{4+}, for a mean oxidation state of 3.3).[22] In contrast, when M = Cu^{2+}, Zn^{2+}, and Sc^{3+}, the variation of T_c with x is not linear and becomes significantly larger than those in the above cases (up

(22) Shannon, R. D. *Acta Crystallogr. A* **1976**, *32*, 751.

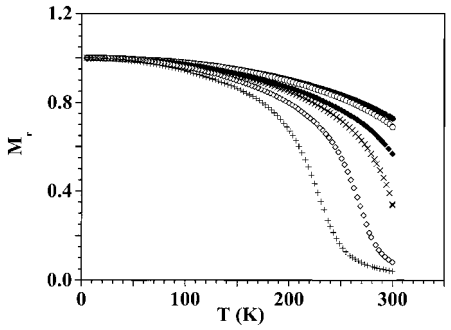

Figure 2. Thermal variation of the reduced magnetization, M(H, T)/M(H, 0 K) for $La_{0.7+y}A_{0.3-y}Mn_{1-x}Cu_xO_3$ (H = 10 kOe; ●, ○, ◆, ×, ◇, and + correspond to data for x = 0.00, 0.02, 0.04, 0.06, 0.08, and 0.10, respectively).

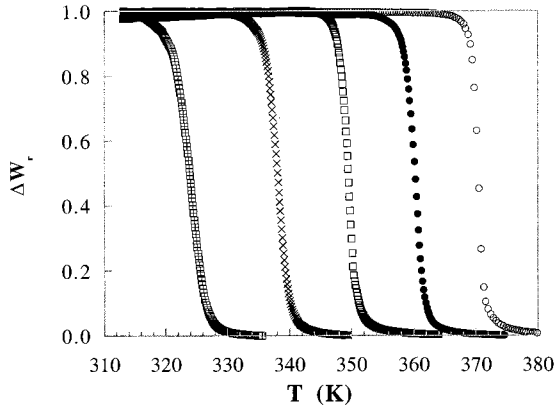

Figure 3. Thermal variation of the normalized force for $La_{0.7+y}A_{0.3-y}Mn_{1-x}Cr_xO_3$ (except the x = 0.10 sample). Values of weight gains below T_c are typically in the 2−4% range. Such a dispersion can be attributed to differences in the sample geometries. Then, the experimental values have been normalized to facilitate the comparison. ○, ●, □, ×, and box with + correspond to data for x = 0.00, 0.02, 0.04, 0.06, and 0.08, respectively.

Table 2. Observed T_c (K) for $La_{1-y}A_yMn_{1-x}M_xO_3$

	x =					
M	0.00	0.02	0.04	0.06	0.08	0.10
			A = Sr			
Cr	372	363	351	340	327	316
Co		355	345	331	312	300
Ga		360	342	329	320	310
Cu		358	331	308	274	236
Zn		350	326	284	233	179
Sc		343	314	280	240	195
			A = Ba			
Cu	330	318	296	260	221	183
Zn		324	286	227	186	162
Sc		296	258	216	184	168

to 52% for Zn^{2+}). Interestingly, the ionic radii of Cu^{2+}, Zn^{2+}, and Sc^{3+} (87, 88, and 88.5 pm, respectively) are, in turn, significantly larger than the mean radius of Mn ions. As might be expected, Ba derivatives behave similarly to their Sr analogues.

Discussion

Unlike the ideal cubic structure, the rhombohedral perovskite presents an irregular 12-coordination around A cations and a B−O−B angle that deviates substantially from 180°. Lattice effects on electronic properties

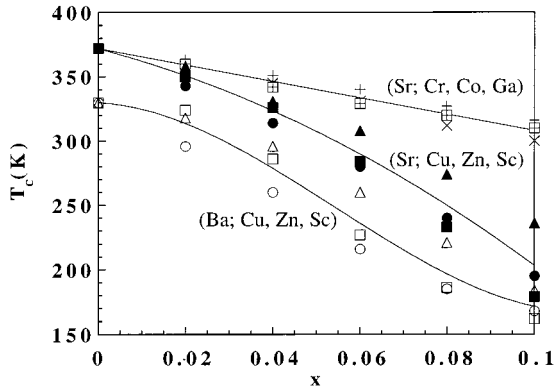

Figure 4. T_c values versus concentration of substitutional defects at the B sites, x, for the $La_{0.7+y}A_{0.3-y}Mn_{1-x}M_xO_3$ series (A = Sr, +, box with +, ×, ▲, ●, and ■ correspond to Cr, Ga, Co, Cu, Sc, and Zn series, respectively; A = Ba, Δ, ○, and □ correspond to Cu, Sc, and Zn series, respectively; solid lines are guides for the eye).

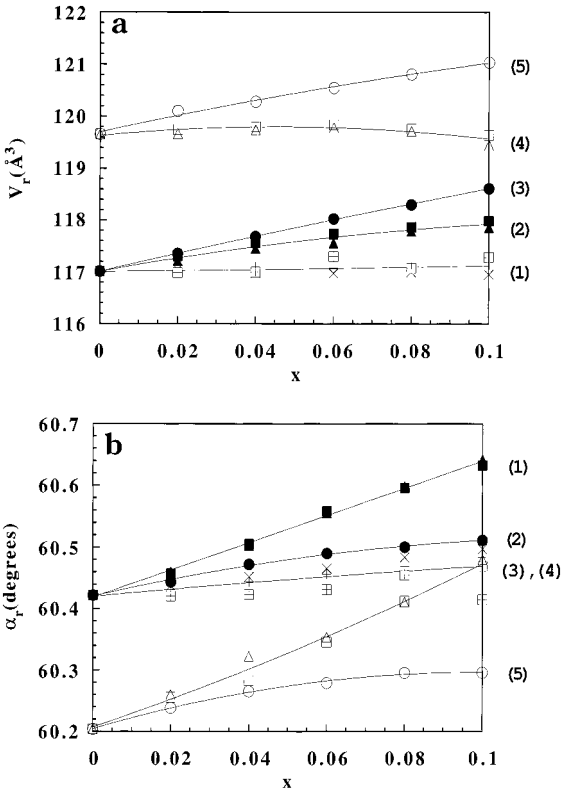

Figure 5. (a) Rhombohedral cell volume, V_r, and (b) rhombohedral cell angle, α_r, versus composition for $La_{0.7+y}A_{0.3-y}Mn_{1-x}M_xO_3$. Data symbols are as in Figure 4. Solid lines are guides for the eye.

of mixed-valence manganates are particularly documented,[5] and we will deal with them first. Figure 5a shows the relationship between the rhombohedral cell volume, V_r, and the composition, x, for the Ba and Sr derivatives in the $La_{1-y}A_yMn_{1-x}M_xO_3$ series. V_r values fit in well with five different curves, which correspond (from bottom to top) to the following series: (1) A = Sr and M = Cr, Co, and Ga; (2) A = Sr and M = Cu and Zn; (3) A = Sr and M = Sc; (4) A = Ba and M = Cu and Zn; (5) A = Ba and M = Sc. In the first case (curve 1), V_r remains practically constant with x, as expected from the similarity among the ionic radii of the dopant cations and the mean radius of the Mn ions and taking

into account the small variation of y along these series (Table 1). In the series in which A = Sr and M = Cu, Zn, and Sc, V_r increases with x (curves 2 and 3). This is reasonable in light of the relatively large size of the dopant cations with respect to the Mn ions. The fact that V_r values adjust to two different curves must be attributed to the different variation of y (which depends on the charge of the substitutional cation) between the Cu and Zn series and the Sc series (Table 1), taking into account that, although similar, $r_{La} < r_{Sr}$. According to this simple reasoning, it can be expected that V_r increases with x more quickly in the Sc series (curve 3) than it does in the Cu and Zn series (curve 2), as is observed. This same reasoning could explain the observation of different behaviors between the A = Ba and M = Cu and Zn series (curve 4) and the A = Ba and M = Sc series (curve 5). On the other hand, the great difference between the ionic radii of La^{3+} and Ba^{2+} allows one to understand that V_r varies smoothly along the Cu and Zn series.

Figure 5b shows the variation of the rhombohedral angle, α_r, with x. Departure of α_r from 60° is a measure of the rhombohedral distortion with respect to the ideal cubic structure. Five different behaviors (as represented by different plots) are again observed, and these correspond to the same series as that in the case of V_r. In fact, as the results suggest, there are the same factors influencing V_r (i.e., relative size of the cations at the A and B sites with respect to the sizes of $La^{3+}$and Mn ions; variation of y with the charge of the substitutional cations at Mn sites) which must affect the structural distortion. Let us argue in terms of the tolerance factor, t,

$$t = d_{A-O}/\sqrt{2}d_{B-O}$$

where d_{A-O} and d_{B-O} are the A−O and B−O bond lengths, with departure of t from unity being a measure of the structural distortion with respective to the ideal perovskite. First, taking into account the sizes of the involved ions, it can be expected that Sr-containing derivatives display higher structural distortions than those of Ba for an analogous content in a given substitutional M cation. On the other hand, the variation of y (Table 1) is significantly higher in the case of substitutional M divalent cations (Cu and Zn) than in the case of trivalent ones (Sc, Cr, Co, and Ga). Therefore, in both Sr and Ba families, t must decrease with x more quickly for the Cu and Zn series. Finally, it is true that the variation of y is the same along all of the Sr-containing series that include trivalent substitutional cations (Cr, Co, Ga, and Sc). However, Sc ions are significantly greater than Cr, Co, and Ga ions. Thereby, it seems reasonable that the increase of α_r in the Sc series is found to be larger than that in the Cr, Co, and Ga series.

Parts a and b of Figure 6 show the dependence of d_{B-O} and d_{A-O}, respectively, on x. Interestingly, the d_{B-O} value sets fit in well with only three different curves. These correspond to the following series: (1) A = Sr and M = Cr, Co, and Ga; (2) A = Sr and M = Cu, Zn, and Sc; (3) A = Ba and M = Cu, Zn, and Sc. Without prejudice from the expected d_{B-O} differences between the Sr and Ba derivatives, it seems evident that the different sizes of the substitutional cations at B sites determine the observed behavior. In contrast, five

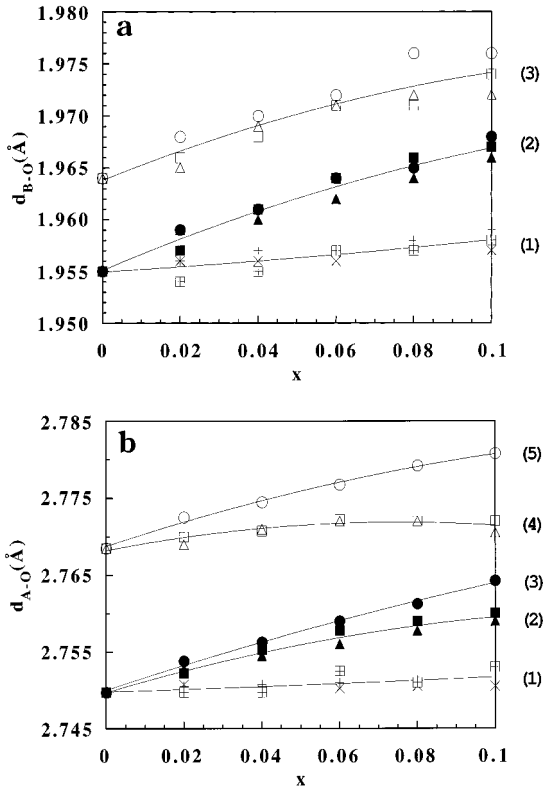

Figure 6. (a) B−O bond length, d_{B-O}, and (b) A−O bond length, d_{A-O}, versus composition for $La_{0.7+y}A_{0.3-y}Mn_{1-x}M_xO_3$. Data symbols are as in Figure 4. Solid lines are guides for the eye.

different curves are required to adjust the experimental d_{A-O} values. In short, it can be concluded that there is the mean size of cations at the B sites which determines the B−O bond length values, whereas the A−O bond lengths depend on the mean sizes of cations at both the A and B sites.

We can now return to the above observations about the dependence of T_c on x. Dealing with Sr derivatives, we have noted that such dependence responds to two different patterns. It might initially be thought that this different behavior is due to differences in the variation of the perovskite tolerance factor, t, as a function of the nature of the substitutional M cation. Shown in Figure 7 is a representation of T_c vs t. As far as the sizes of Cr, Co, and Ga ions are similar to the mean size of Mn cations, the variation of the t values attributable to the substitutional M cation must be small, however, along these series. In fact, the main contribution to the slight decrease of t with x in these series should be associated with the coupled substitution at A sites (La^{3+} instead of Sr^{2+}). Therefore, the observed experimental variation of T_c in these series would essentially reflect the effect of introducing dopant atoms in the B cationic sublattice, with this effect being modulated by the magnetic moment of the impurity. The situation changes when dealing with large substitutional M cations, namely, Cu, Zn, and Sc. Now, besides the effects associated with the B sublattice variations, an additional contribution to the T_c decrease with x, which is associated with the concomitant decrease of t (because of the range of variation of t values throughout these series), can also be expected. However, the experimental variation of T_c in the case of the Ba-containing derivatives is clearly in

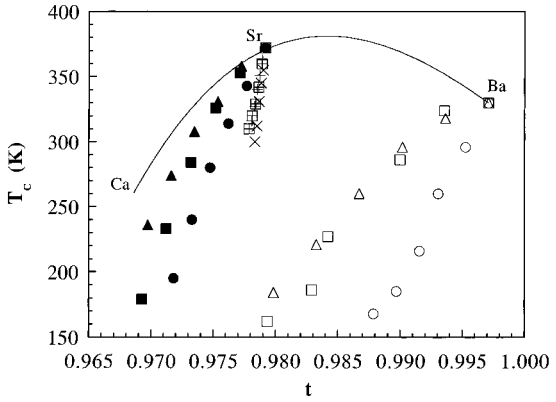

Figure 7. T_c values versus tolerance factor of the perovskite structure, t, for the $La_{0.7+y}A_{0.3-y}Mn_{1-x}M_xO_3$ series (data symbols are as in Figure 4; the solid line has been constructed from data corresponding to the $La_{0.7}(Ca_{1-x}Sr_x)_{0.3}MnO_3$ series , x = 0.00, 0.20, 0.40, 0.60, 0.80, and 1.00, and the $La_{0.7}Ba_{0.3}MnO_3$ sample). Tolerance factors, t, are calculated from the mean radii of cations in A and B positions, $\langle r_A \rangle$ and $\langle r_B \rangle$. $\langle r_A \rangle$ and $\langle r_B \rangle$ values are calculated as the weighted average of crystal radii of cations occupying A and B positions, for coordination numbers 12 and 6, respectively; values are taken from data reported in ref 22.

contradiction to this preliminary approach. In effect, as is evident from Figure 7, given the range of t values corresponding to samples in the Ba series, it could be expected a priori that the decrease of t due to the coupled substitution would result now in a concomitant increase of T_c. However, such a contribution to increasing T_c would work against the expected T_c decrease associated with the introduction of substitutional cations in the B sublattice. Thus, it seems reasonable that both counterweighting effects would give rise to only a slight variation of the T_c values. In contrast, the experimental T_c variation along the Ba series is very large, thus suggesting that there are other factors controlling the dependence of T_c on x (at least in the Cu, Zn, and Sc series).

From the above, it seems that the use of mainly structural factors, like t, is unable to explain by itself the described phenomenology. In practice, such an approach could be undervaluing local effects associated with the introduction of so differently sized impurities, which must result in different perturbations of the periodic potential seen by the electrons in the vicinity of the substitutional defects. Indeed, we have explored an alternative approach that fully assumes the relevance of these local effects. It is a question of considering how the presence of these local effects affects the electronic contribution to the transition enthalpy, ΔH_e, and, therefore, the electronic contribution to the critical temperature, T_e.[11]

In accordance with the theoretical approach of Sheng et al.,[23] the electronic contribution to the transition enthalpy (and, consequently, $T_e \approx \Delta H_e/\Delta S$; $\Delta S \approx \Delta S_m$, where ΔS_m is the magnetic entropy) is mainly caused by the spin dependence of the transfer integral, t_{ij}, which can be written as $t_{ij} = b \cos(\theta_{ij}/2)$, where b is the spin-independent transfer integral and θ_{ij} is the angle

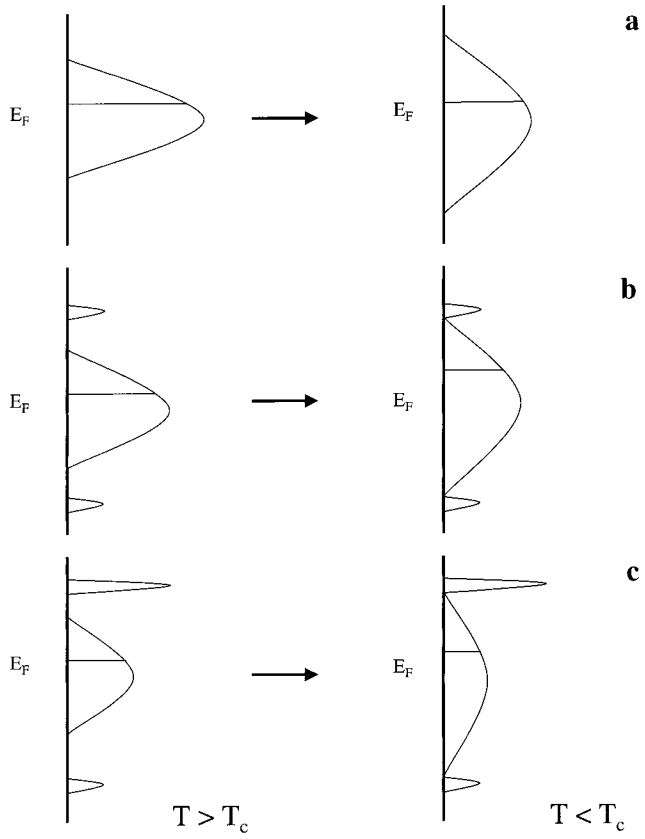

Figure 8. Densities of states (DOS) of the conduction band in mixed-valence manganates, for temperatures below and above T_c: (a) no structural disorder; (b) situation with structural disorder produced by substitutional defects with size similar to the mean size of Mn ions; (c) situation with structural disorder produced by large substitutional defects.

between spins on neighboring Mn atoms. Within this model, the electronic contribution to the transition enthalpy can be approximated by

$$\Delta H_e = E_{PM} - E_{FM} \approx \int \mathrm{DOS}_{PM}(E)\, f(E-\mu_{PM})\, E\, \mathrm{d}E - \int \mathrm{DOS}_{FM}(E)\, f(E-\mu_{FM})\, E\, \mathrm{d}E \quad (1)$$

where PM and FM represent the paramagnetic and ferromagnetic phases, respectively, E_{FM} and E_{PM} are the electronic energies, $\mathrm{DOS}_i(E)$ is the density of states in the conduction band, and $f(E-\mu_i)$ is the Fermi−Dirac distribution function with chemical potentials μ_i, determined from the condition of fixed hole concentration.[23] The conduction band in mixed-valence manganates is an antibonding σ^* band of e_g orbital parentage. In the absence of structural disorder, the spin order is maximum in the FM phase, and the width of the conduction band is $W_{FM} = 12b$. As the temperature increases, the spin disorder increases slowly until T_c, and then it increases abruptly, being maximum in the PM phase. The width of the conduction band in the PM phase is $W_{PM} = 8b$.[24] The electronic structure in the vicinity of the Fermi level can be schematized, for the PM and FM phases, as shown in Figure 8a. The zero in the energy scale is taken at the middle of the bands. Then, the band

(23) (a) Sheng, L.; Xing, D. Y.; Sheng, D. N.; Ting, C. S. *Phys. Rev. Lett.* **1997**, *79*, 1710. (b) Sheng, L.; Xing, D. Y.; Sheng, D. N.; Ting, C. S. *Phys. Rev. B* **1997**, *56*, 7053.

(24) Li, Q.; Zhang, J.; Bishop, A. R.; Soukoulis, C. M. *Phys. Rev. B* **1997**, *56*, 4541.

edges corresponding to the PM and FM phases are located at $\pm 4b$ and $\pm 6b$, respectively. The presence of disorder will cause a fraction of the states in the conduction band to become located beyond the original band edges, in energy intervals defined by $\pm[6b, 6b + W/2]$ for both PM and FM phases, where W is the disorder energy (Figure 8b). When these ideas are taken as the starting point, it is clear that substitutional defects in the B cationic sublattice introduce different types of disorder, depending on the size of the substitutional cations. If this last one is similar to the mean size of Mn ions, the structural disorder introduced in the lattice would be very low, and should be equally able to locate electrons below the bottom of the band and holes above the top of the band (Figure 8b). However, the structural disorder is very high when the substitutional cations have a large size compared to that of Mn. The strong local stress produced by these defects can be alleviated in two different ways. First, it can be expected that MO_6 octahedra rotate in association with rotations of the neighboring octahedra. Second, the local stress can also be alleviated by a decrease in the Mn−O bond lengths of the Mn−O−M linkages, as far as the Mn−O bonds of the neighboring Mn ions are under compression. Thus, the substitutional defects introduce a local source of internal pressure. Rotations of the MnO_6 octahedra neighboring substitutional M atoms will modify (reduce) the Mn−O−Mn angles and, thus, a decrease in the mean transfer integral must be expected. However, more importantly, the decrease of the Mn−O bond lengths in the Mn−O−M linkages results in a preferred trapping of the holes at these neighboring Mn positions. Thus, together with the tendency to locate both electrons and holes beyond band edges, because of the presence of a random distribution of substitutional defects, this kind of disorder should be able to locate strongly holes above the top of the band (Figure 8c).

Let us assume that the distribution of states beyond the band edges is independent of the ordering of the magnetic moments and that the form of the DOS curve inside the band edges is not substantially modified by the disorder. Then, if y is the fraction of states located beyond the band edges, we can write

$$\mathrm{DOS}_{i,\mathrm{D}}(E) = (1 - y)\mathrm{DOS}_{i,\mathrm{O}}(E) \qquad i = \mathrm{PM, FM} \qquad (2)$$

where $\mathrm{DOS}_{i,\mathrm{D}}(E)$ and $\mathrm{DOS}_{i,\mathrm{O}}(E)$ are the densities of states in the i phase for the disordered (D) and ordered (O) cases, respectively, in the energy interval $-6b \le E \le 6b$. Under this assumption, the condition

$$T_{\mathrm{e,D}} = (1 - y)T_{\mathrm{e,O}} \qquad (3)$$

is easily derived from eq 1.

The effect of structural disorder is, therefore, to reduce the electronic contribution, T_e, to the critical temperature, T_c. Other factors being equal, the fraction of states located beyond the band edges will increase as the disorder energy, and, consequently, T_e decrease. It is clear that, under these assumptions, the marked decrease in the critical temperature in the case of large substitutional cations has its origin in their strong tendency to locate holes at the top of the band.

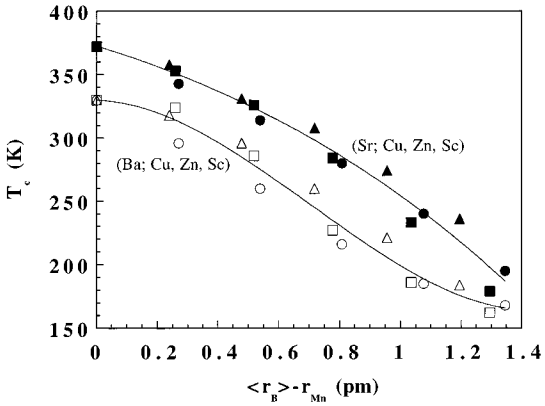

Figure 9. T_c values versus degree of disorder, measured by $\langle r_B \rangle - r_{Mn}$ (see text) for Sc, Cu, and Zn strontium series. Data symbols are as in Figure 4.

This description also provides an explanation for the previously observed decrease in T_c as a consequence of an increasing concentration of vacancies at B sites.[13] In effect, in a Mn−O−Mn linkage, the Mn−O bond distances are the result of the interaction of both manganese cations with the oxygen anion. However, in Mn−O−V_{Mn} linkages, the Mn−O distance is the result of the interaction of only one Mn cation with the oxygen anion and, thus, the Mn−O distance must be lower than that in the Mn−O−Mn linkage. Therefore, neighboring Mn cations act as trapping centers for holes, and a decrease in T_c follows from the increase in the concentration of vacancies at B sites.

Last, in the case of Mn substitutional defects, the degree of structural disorder introduced by large substitutional cations (and, thus, the fraction of states located at the top of the band) must be proportional to (1) the concentration of the substitutional metal, x, and (2) the difference between the size of the substitutional metal and the mean size of the Mn ions ($r_M - r_{Mn}$). If so, it is straightforward to deduce that $x(r_M - r_{Mn}) = \langle r_B \rangle - r_{Mn}$, where $\langle r_B \rangle$ is the mean size of cations at the B positions. Shown in Figure 9 is the variation of T_c versus the degree of structural disorder introduced by the large substitutional cations, as measured by $\langle r_B \rangle - r_{Mn}$, for the Cu^{2+}, Zn^{2+}, and Sc^{3+} series. As can be observed, there is a very good correlation between T_c and $(\langle r_B \rangle - r_{Mn})$. Such a result indicates that (1) the decrease in T_c is mainly determined by the local effect of the structural disorder introduced by large substitutional cations and (2) it is poorly modulated by the magnetic nature of the substitutional metals (Cu^{2+} versus Zn^{2+} and Sc^{3+}) or by the different stoichiometries of the samples (Sc^{3+} versus Cu^{2+} and Zn^{2+}). In any case, it is clear that this variation must include the contribution of the decrease in t associated with these substitutions.

Concluding Remarks

Introduction of substitutional cations at B sites has been one of the methods used in order to modify the intrinsic properties of CMR $La_{1-x}A_xMnO_3$ perovskites. In particular, such a procedure has been explored in order to improve the room-temperature low-field sensitivity of these materials (thin films) for applications

in magnetic sensors.[25] We have shown how the electronic properties of mixed-valence manganates with defects in the B cationic sublattice are controlled by the structural disorder introduced by the local internal pressure associated with large substitutional defects. Our results indicate that the size of the substitutional cations is a key parameter in the maintenance of the critical temperature around room temperature, which could be a guide for the adequate selection of CMR materials.

Acknowledgment. F.S. thanks R. J. Ortega and D. Beltrán for valuable discussions. Z.E.-F. is grateful to the Spanish Instituto de Cooperación con el Mundo Arabe, the Universitat de València, and the Spanish Ministerio de Ciencia y Tecnología for grants. The Spanish Comisión Interministerial de Ciencia y Tecnología (CICYT; MAT96-1037 and MAT99-6481) and the European Union (European Network SUPER-GMR) supported this work.

Supporting Information Available: Tables of refined structural parameters and residuals and selected lists of bond distances and angles, as well as cell parameters, for the rhombohedral setting (PDF). This material is available free of charge via the Internet at http://pubs.acs.org.

CM010655E

(25) Obata, T.; Tsuge, H.; Shohata, N. U.S. Patent 5,681,500, 1997.